American Journal of Applied Mathematics
2026, Vol. 14, No. 3, pp. 148–159
https://doi.org/10.11648/j.ajam.20261403.15

Research Article

# Cross-Diffusion Impacts on Jeffrey Nanofluid Flow in a Lorentz Force–Driven Stretchable Channel with Nonlinear Radiation

**Sunitha Manchaiah Savithramma[1], Kemparaju Siddegowda[2,*], Jagadeesha Ragibychanahalli Devaraju[3], Sampath Kumar Poojari Borappa[4]**

[1]Department of Mathematics, Government First Grade College, Tumkur, India
[2]Department of Mathematics, Government First Grade College, Ramanagara, India
[3]Department of Mathematics, Government First Grade College for Women, Holenarasipura, India
[4]Department of Mathematics, Ramanagara PG Centre, Ramanagara, India

## Abstract

This study investigates the three-dimensional flow and heat transfer characteristics of a Jeffrey nanofluid flowing through a stretching channel under the influence of a Lorentz force generated by an applied magnetic field. The Jeffrey fluid model is a significant non-Newtonian fluid model that accounts for both relaxation and retardation effects, which are important in describing the viscoelastic behavior of complex fluids. The incorporation of magneto-hydrodynamic (MHD) effects enables the analysis of electrically conducting fluids subjected to magnetic forces, which are widely encountered in industrial and engineering applications such as cooling systems, polymer processing, and biomedical devices. The analysis further considers nonlinear thermal radiation to accurately represent heat transfer at high temperature conditions. In addition, the Soret and Dufour effects are included to examine cross-diffusion phenomena between heat and mass transfer processes. The Soret effect describes mass diffusion caused by temperature gradients, whereas the Dufour effect represents energy flux generated due to concentration gradients. These coupled transport mechanisms significantly influence the thermal and concentration boundary layers. The governing nonlinear PDEs are transformed into ODEs using suitable similarity transformations and solved numerically. The effects of various controlling physical parameters on velocity, temperature, and concentration distributions are examined in detail. The numerical results reveal that an increase in the Dufour number enhances thermal energy transport, leading to higher temperature and velocity profiles while reducing concentration distribution. Conversely, increasing the Soret number strengthens mass diffusion induced by temperature gradients, thereby improving concentration and velocity distributions within the boundary layer region.

## Keywords

Cross-diffusion, Jeffrey Fluid, Convection, Thermal Radiation

*Correspondence: Kemparaju Siddegowda (skemparaju74@gmail.com)

**Received:** 6 May 2026; **Accepted:** 16 May 2026; **Published:** 25 June 2026

# 1. Introduction

When considering multi-component fluid systems, temperature and concentration gradients may appear to be independent, and in some instances, interact through coupled transport mechanisms also known as cross-diffusion effects. The Soret effect illustrates how a heat gradient separates species in a mixture. In the opposite case, the Dufour effect describes the case where concentration gradients, in combination with the energy equation, create an additional heat flux that changes the thermal energy transport of the fluid. When it comes to strong thermal gradients, reactive mixtures, or magnetohydrodynamic environments, these interdependent mechanisms become more crucial. They may be important in the design of polymer processing, chemical reactors, geothermal systems, and in the flow of fluids in space. Many models of fluid flow have included cross-diffusion mechanisms to capture the heat and mass transfer and understand their role. For example, Turkyilmazoglu and Pop [1] studied mass thermally induced diffusion and diffusion-thermo effects in viscous flow caused by the Lorentz force over a flat plate. Zheng et al. [2] carried that study to hydromagnetically viscous flow over oscillatory stretching surfaces and noted the influence cross-diffusion had on the flow. In [3] Reddy and Chamkha examined the effects of some of the mechanisms described previously in magnetized nanofluids and revealed significant changes in the thermal and concentration fields. Sampath Kumar et al. [4] carried out a nonlinear analysis of Jeffrey fluid flow in thermal convection under cross-diffusion and boundary convective circumstances. Hayat et al. [5] examined three-dimensional conductive flows with radiative influences, whereas Zia et al. [6] examined Casson fluid flow cross-diffusion effects with internal heat production, thermal radiation, and heat creation. Madan Kumar et al. [7] used Darcy's equations to calculate stable two-dimensional Jeffrey fluid flows across a stretched porous material and included thermal diffusion and diffusion-thermo effects. Subhan Ullah et al. [8] examined Joule heating, chemical reaction, heat sink, cross-diffusion, and hydromagnetic Jeffrey-Hamel flows in converging and diverging stretchable channels. They reported that heat sources and Dufour parameters increase temperature profiles, while Soret effects reduce concentration. Due to their relevance to engineering and applied sciences, the cross-diffusion effects have also received much attention in the related works studies [9-12], indicating the relevance to advanced transport modelling.

A pair stress fluid in a conduit with one electrically conducting wall and one non-conducting wall undergoes thermal diffusion and diffusion-thermo influenced magnetohydrodynamic double-diffusive mixed convection, according to Shilpa et al. [13]. Mair et al. [14] studied entropy formation in Bingham plastic fluid incompressible boundary layer flow across an inclined, rough, rotating disk. The research examined how cross-diffusion and radiative heat flow affect thermal and mass movement. Under velocity slip circumstances, Surbhi et al. [15] quantified the effects of melting, thermal diffusion, and diffusion-thermo on Casson fluid flow over a stretched surface. Their results indicated that increasing the Dufour parameter enhances the temperature distribution, and a similar rising trend in thermal profile was observed with higher values of the Soret number.

Nuclear reactor cooling, thermal storage devices, refrigeration, electronic cooling, solar energy harvesting, and many other thermal engineering systems rely on natural, forced, and mixed convective heat transport. The versatility of convection-driven flows has led to their investigation in a wide range of physical settings and fluid models by Gorla and Sidawi [16] and also they explored buoyancy-induced flow across a stretched elastic surface with transpiration, whereas Wang [17] studied mixed convection heat transfer of non-Newtonian fluids on vertical surfaces. Chamkha [18] investigated stretched plate hydromagnetic natural convection, Rashidi et al. [19] explored micropolar fluid mixed convection boundary-layer flow utilizing homotopy analysis, and Giressha [20] studied Maxwell fluids with suspended particles, nonlinear radiation, and non-uniform heat source. Numerous studies have explored convection in different configurations [21-24]. Many investigations have employed linear thermal convection's persistence for very tiny temperature changes. Large temperature changes affect buoyancy-driven flows in solar collectors, electronic cooling devices, nuclear reactors, and energy storage devices, generating non-linear density-temperature correlations. Vajravelu et al. [25], Kameswaran et al. [26], and Sachin et al. [27] explored nonlinear convection's effects to address this. Recently, Jyoti et al. [28] Magammad et al. [29] Studied buoyancy-driven nonlinear coupled convection with radiative effects over a non-Newtonian fluid-stretching vertical sheet and heat radiation in kerosene-alumina nanofluid flow between parallel plates with variable vis/vis. A base fluid with microscopic solid particles forms nanofluids, which increase thermophysical characteristics. Krishnan [30] conducted a rheometric analysis where he showed that temperature, the volume fraction and mass of nanoparticles, remarkably affect the viscosity of water-based nanofluids. A study by Sampath et al. [31] showed better thermal performance of Cu and $Fe_3O_4$ nanofluids in the case of convective heat transfer. In addition, Nishandar et al. [32] showed that $Al_2O_3$, CuO, and hybrid nanofluids are quite useful in improving the efficiency of vapour compression refrigeration. Gunisetty et al. [33] investigated magnetized Casson nanofluid blood flow through a stenotic artery and reported that increasing magnetic field strength reduces blood velocity, while copper nanoparticles enhance heat transfer and may improve targeted drug delivery within the circulatory system. Gunisetty and Balaanki [34] performed a numerical analysis on the influence of multiple nanoparticle shape factors in Casson hybrid nanofluid flow over a rotating disk and reported significant variations in thermal transport characteristics due to particle geometry effects. Ramasekhar [35] investigated magnetohydrodynamic hybrid

nanofluid flow over a stretching cylinder using artificial neural network techniques and numerical simulations to analyze complex thermal transport behavior.

Magnetohydrodynamic (MHD) nanofluid flow has gained considerable attention due to its wide range of applications in engineering and industrial processes, including cooling systems, thermal energy storage, nuclear reactors, metallurgical processing, and biomedical technologies. The suspension of nanoparticles in conventional base fluids significantly enhances thermal conductivity and improves heat transfer characteristics, while the application of an external magnetic field provides an effective mechanism for controlling the motion and thermal behavior of electrically conducting fluids. In high-temperature thermal systems, thermal radiation plays a crucial role in the energy transport process, and the nonlinear radiation model offers a more realistic description of thermal behavior compared with linearized radiation approximations, especially in situations involving large temperature differences. Owing to these important practical applications and enhanced thermal transport characteristics, several researchers have recently investigated MHD nanofluid flow in the presence of nonlinear thermal radiation effects [36-41].

Engineering has many uses for Jeffrey fluids as viscoelastic models in non-Newtonian fluids. Some fields of engineering that use Jeffrey fluids in modelling include: Biomedical engineering, lubricant engineering, and design of thermal systems. Jeffrey fluids model relaxation and retardation in Dalir [42], Qasim [43], Shehzad et al. [44], Ramesh [45], Veera Krishna and Chamkha [46]. Researchers in magneto-hydrodynamics assume the fluid acts linearly according to Newtonian thermal theory. Constraints like this are often used in modeling. This work aims to fill a gap in the literature by investigating poorly understood phenomena such as thermophoretic fluid flow over vertical surfaces, nonlinear convection, cross-diffusion, and mixed-mode hydrodynamics (MHD). Deepening our understanding of fluid-dependent engineering processes is the overarching objective of this study.

## 2. Mathematical Formulation

Consider the two-dimensional Jeffrey fluid boundary layer flow begun by a linearly stretched sheet at "$y = 0$", with the fluid occupying the region "$y > 0$". Equal and opposing forces stretch the surface along the x-direction, creating a linear velocity profile. $U_w = ax$, where $a$is a positive constant. The x-axis is chosen to be perpendicular to the stretching surface, and the y-axis is aligned with it in the Cartesian coordinate system. At the surface, convective heating and mass transfer are imposed, characterized by the surface temperature $T_f$ and concentration $C_f$, along with the corresponding heat and mass transfer coefficients $h_1$and $h_2$. The fluid nears temperature uniformity away from the sheet ($T_\infty$) and concentration $C_\infty$. Using this physical model, we may study the linked thermal and solutal transport in a stretching-surface-moving Jeffrey fluid. The following equations regulate the issue under investigation (see Hayat et al. [36], Sachin et al. [27]);

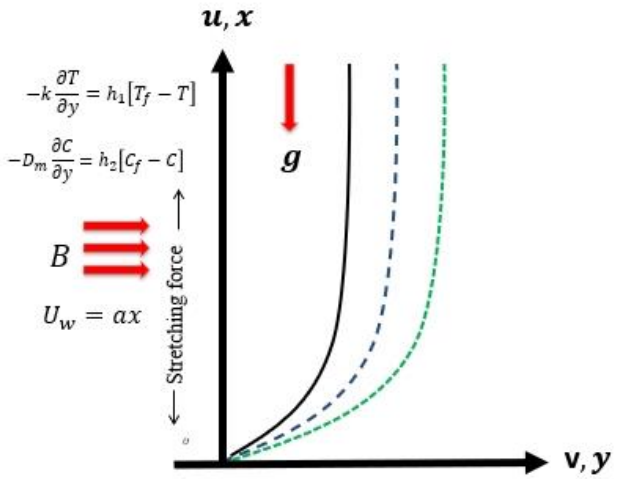


***Figure 1.*** *Mathematical flow geometry.*

$$\frac{\partial u}{\partial x} + \frac{\partial v}{\partial y} = 0, \tag{1}$$

$$u\frac{\partial u}{\partial x} + v\frac{\partial u}{\partial y} = \left(\frac{\nu}{1+\lambda_1}\right)\left[\frac{\partial^2 u}{\partial y^2} + \lambda_2\left(u\frac{\partial^3 u}{\partial x \partial y^2} + v\frac{\partial^3 u}{\partial y^3} - \frac{\partial u}{\partial x}\frac{\partial^2 u}{\partial y^2} + \frac{\partial u}{\partial y}\frac{\partial^2 u}{\partial x \partial y}\right)\right] - \frac{\sigma B^2}{\rho}u + g(\beta_0(T - T_\infty) + \beta_1(T - T_\infty)^2 + \beta_2(C - C_\infty)), \tag{2}$$

$$u\frac{\partial T}{\partial x} + v\frac{\partial T}{\partial y} = \alpha_m\frac{\partial^2 T}{\partial y^2} + \frac{D_m K_T}{C_s C_p}\frac{\partial^2 C}{\partial y^2} + \tau\left[\mathrm{D_m}\left(\frac{\partial \mathrm{C}}{\partial y}\frac{\partial \mathrm{T}}{\partial y}\right) + \frac{\mathrm{D_T}}{\mathrm{T_\infty}}\left(\frac{\partial \mathrm{T}}{\partial y}\right)^2\right] - \frac{1}{\rho c_p}\frac{\partial q_r}{\partial y} + \frac{Q_0}{\rho c_p}(T - T_\infty) + \frac{\mu}{\rho C_p(1+\lambda_1)}\left[\left(\frac{\partial u}{\partial y}\right)^2 + \lambda_2\left(u\frac{\partial u}{\partial y}\frac{\partial^2 u}{\partial x \partial y} + v\frac{\partial u}{\partial x}\frac{\partial^2 u}{\partial y^2}\right)\right], \tag{3}$$

$$\frac{\partial C}{\partial x} + v\frac{\partial C}{\partial y} = \left[D_m\left(\frac{\partial^2 C}{\partial y^2}\right) + \frac{D_T}{T_\infty}\frac{\partial^2 T}{\partial y^2}\right] + \frac{D_m K_T}{T_m}\frac{\partial^2 T}{\partial y^2} - \frac{\partial(V_T C)}{\partial y}, \tag{4}$$

The radiative heat flux expression in equation (3) is given by the Rosseland approximation as;

$$q_r = -\frac{4\sigma^*}{3k^*}\frac{\partial T^4}{\partial y} = -\frac{16\sigma^*}{3k^*}T^3\frac{\partial T}{\partial y}, \tag{5}$$

Where σ* and k* are the Stefan-Boltzman constant and the mean absorption coefficient correspondingly, and in view to equation (5) in equation (3) reduces to;

$$u\frac{\partial T}{\partial x}+v\frac{\partial T}{\partial y}=\alpha_m\frac{\partial^2 T}{\partial y^2}+\frac{D_mK_T}{C_sC_p}\frac{\partial^2 C}{\partial y^2}\tau\left[\mathrm{D}_m\left(\frac{\partial \mathrm{C}}{\partial y}\frac{\partial \mathrm{T}}{\partial y}\right)+\frac{\mathrm{D_T}}{\mathrm{T}_\infty}\left(\frac{\partial \mathrm{T}}{\partial y}\right)^2\right]+\frac{16\sigma^*}{3\rho c_p k^*}\left[T^3\frac{\partial^2 T}{\partial y^2}+3T^2\left(\frac{\partial T}{\partial y}\right)^2\right]+\frac{Q_0}{\rho c_p}(T-T_\infty)+\frac{\mu}{\rho C_p(1+\lambda_1)}\left[\left(\frac{\partial u}{\partial y}\right)^2+\lambda_2\left(u\frac{\partial u}{\partial y}\frac{\partial^2 u}{\partial x\partial y}+v\frac{\partial u}{\partial x}\frac{\partial^2 u}{\partial y^2}\right)\right], \quad (6)$$

The corresponding boundary conditions at the surface and far away from the surface are written as follows;

$$u=U_w(x), v=-V_w(x), -k\frac{\partial T}{\partial y}=h_1(T_f-T), -D_m\frac{\partial C}{\partial y}=h_2(C_f-C) \text{ at } y=0,$$

$$u\to 0, \frac{\partial u}{\partial y}\to 0, T\to T_\infty, C\to C_\infty \text{ as } y\to\infty, \quad (7)$$

$\nu$ represents dynamic viscosity, while $u$ and $v$ indicate velocity components along the x- and y-axes, $\lambda_1$ and $\lambda_2$ representing relaxation and retardation times, $g$ representing gravity acceleration, $B$ representing magnetic field, $T_m$ representing fluid mean temperature, $\beta_2$ representing volumetric solute expansion coefficient, and $\beta_0$ and $\beta_1$. The coefficients for volumetric thermal expansion are $\alpha_m$ (thermal diffusivity), $D_m$ (solutal diffusivity), $\rho$ (density), $K_T$ (thermal diffusion ratio), $C_s$ (concentration susceptibility), $C_p$ (specific heat capacity), $\mu$ (dynamic viscosity), $Q_0$ (heat generation/absorption coefficient), $V_T$ (thermophoretic velocity), and k (thermal conductivity). T = fluid temperature, C = concentration, $\mathrm{T}_\infty$ = ambient temperature and $C_\infty$- ambient concentration. The term $V_T$ in equation (4) can be defined as follows;

$$V_T=-k_1\frac{\nu}{T_r}\frac{\partial T}{\partial y}, \quad (8)$$

here $k_1$ - thermophoretic coefficient and $T_r$ -reference temperature.

Now, introduce the following similarity transformations

$$\chi=\sqrt{\frac{U_w}{\nu x}}y,\ u=axf'(\eta),\ v=-\sqrt{a\nu}f(\eta),\ \theta(\eta)=\frac{T-T_\infty}{T_f-T_\infty},\phi(\eta)=\frac{C-C_\infty}{C_f-C_\infty},\ T=T_\infty(1+(\theta_w-1)\theta(\eta)) \text{ with } \theta_w=\frac{T_f}{T_\infty},\theta_w>1 \quad (9)$$

Into the equations (2) to (7), we get

$$\frac{d^3f}{d\chi^3}+(1+\lambda_1)\left(f(\chi)\frac{d^2f}{d\chi^2}-\left(\frac{df}{d\chi}\right)^2\right)+\beta\left(\left(\frac{d^2f}{d\chi^2}\right)^2-f(\chi)\frac{d^4f}{d\chi^4}\right)+\lambda(1+\lambda_1)(\theta(\chi)+\alpha\theta(\chi)^2+N\phi(\chi))-(1+\lambda_1)M\frac{df}{d\chi}=0, \quad (10)$$

$$(1+\lambda_1)\left\{\frac{d^2\theta}{d\chi^2}+R\left[\left(1+(\theta_w-1)\theta(\chi)\right)^3\frac{d^2\theta}{d\chi^2}+3(\theta_w-1)\theta'^2(\chi)\left(1+(\theta_w-1)\theta(\chi)\right)^2\right]+\mathrm{Pr}\left(f(\chi)\frac{d\theta}{d\chi}+D_f\frac{d^2\phi}{d\chi^2}+Q\theta(\chi)\right)\right\}+PrEc\left\{\left(\frac{d^2f}{d\chi^2}\right)^2+\beta\frac{d^2f}{d\chi^2}\left(\frac{df}{d\chi}\frac{d^2f}{d\chi^2}-f(\chi)\frac{d^3f}{d\chi^3}\right)\right\}+PrNb\frac{d\theta}{d\chi}\frac{d\phi}{d\chi}+Nt\left(\frac{d\theta}{d\chi}\right)^2=0, \quad (11)$$

$$\frac{d^2\phi}{d\chi^2}+Scf\frac{d\phi}{d\chi}+ScSr\frac{d^2\theta}{d\chi^2}-Sc\tau\left(\frac{d\phi}{d\chi}\frac{d\theta}{d\chi}+\phi\frac{d^2\theta}{d\chi^2}\right)+\frac{Nt}{Nb}\frac{d^2\theta}{d\chi^2}=0, \quad (12)$$

and the corresponding boundary conditions become;

$$f'=1, f=S, \theta'=-Bi_1(1-\theta), \phi'=-Bi_2(1-\phi) \text{ at } \chi=0,$$

$$f'\to 0, f''\to 0, \theta\to 0, \phi\to 0 \text{ as } \chi\to\infty. \quad (13)$$

The following parameters are involved in nonlinear convection: dimensionless mixed convection, buoyancy ratio, magnetic, Dufour, Prandtl, heat generation, radiation, temperature ratio, Eckert, Schmidt, thermophoretic, Soret, suction, thermal Biot, concentration Biot, Brownian motion, electrophoresis;

$$\lambda=\frac{Gr_x}{(Re_x)^2},\ Gr_x=\frac{g\beta_0(T_f-T_\infty)U_w^3}{\nu^2a^3},\ Re_x=\frac{U_w^2}{\nu a},\ \beta=\lambda_2 a,\ \alpha=\frac{\beta_1(T_f-T_\infty)}{\beta_0},$$

$$N=\frac{\beta_2(C_f-C_\infty)}{\beta_0(T_f-T_\infty)},\ M=\frac{\sigma B^2}{\rho a},\ D_f=\frac{D_mK_T(C_f-C_\infty)}{Cs\,C_p\nu(T_f-T_\infty)},\ Pr=\frac{\nu}{\alpha_m},$$

$$Q = \frac{Q_0}{a\rho c_p},\ R = \frac{16\sigma^* T_\infty^3}{3k^* k},\ \theta_w = \frac{T_f}{T_\infty},\ Ec = \frac{U_w^2}{C_p(T_f - T_\infty)},\ Sc = \frac{\nu}{D_m},$$

$$\tau = -\frac{k_1(T_f - T_\infty)}{T_r},\ Sr = \frac{D_m K_T(T_f - T_\infty)}{T_m \nu(C_f - C_\infty)},\ S = \frac{V_w}{\sqrt{a\nu}},\ Bi_1 = \frac{h_1}{k}\sqrt{\frac{\nu}{a}}\ Bi_2 = \frac{h_2}{D_m}\sqrt{\frac{\nu}{a}},$$

$$N_b = \frac{\tau D_m(C_f - C_\infty)}{\nu},\ N_t = \frac{\tau D_T(T_f - T_\infty)}{T_\infty \nu}.$$

The Skin friction coefficient, Nusselt number and Sherwood numbers are;

$$C_f = \frac{\tau_w}{\rho U_w^2}, Nu_x = \frac{xq_w}{k(T_f - T_\infty)}, Sh_x = \frac{xq_m}{D_m(C_f - C_\infty)} \quad (14)$$

By Fourier's law, $\tau_w$ -surface shear stress, $q_w$-surface heat flux and $q_m$ -surface mass flux are given by;

$$\tau_w = \frac{\mu}{1+\lambda_1}\left[\mu\frac{\partial u}{\partial y} + \lambda_2\left(u\frac{\partial^2 u}{\partial x \partial y} + v\frac{\partial^2 u}{\partial y^2}\right)\right]_{y=0},$$

$$q_w = -k\left(\frac{\partial T}{\partial y} + q_r\right)_{y=0},$$

$$q_m = -D_m\left(\frac{\partial C}{\partial y}\right)_{y=0} \quad (15)$$

Now by combining equation (9) and (15) in view of equation (14), we have obtained;

$$C_f Re_x^{1/2} = \frac{1}{1+\lambda_1}(f''(0) + \beta(f'(0)f''(0) - f(0)f'''(0))),$$

$$Nu_x Re_x^{-1/2} = -(1 + R\theta_w^3)\theta'(0),$$

$$Sh_x Re_x^{-1/2} = -\phi'(0) \quad (16)$$

***Table 1.*** *Validation of the computed skin-friction coefficient $f''(0)$ against previously published results of Hayat et al. [36] and Dalir [42] under the special case $S = \lambda = 0$, $\beta = 0.2$, and $Nb = Nt = 0$.*

| $\lambda_1$ | Hayat et al. [36] | Dalir [42] | Present Study (RKF-45) |
|---|---|---|---|
| 0 | -0.91287 | -0.91468 | -0.91299 |
| 0.2 | -1.00000 | -1.00124 | -1.00006 |
| 0.4 | -1.08012 | -1.08100 | -1.08016 |
| 0.6 | -1.15471 | -1.15534 | -1.15472 |
| 0.8 | -1.22474 | -1.22522 | -1.22476 |
| 1.0 | -1.29099 | -11.2913 | -1.29110 |
| 1.2 | -1.35401 | -1.35428 | -1.35401 |
| 1.4 | -1.41421 | -1.41442 | -1.41422 |
| 1.6 | -1.47196 | -1.47212 | -1.47196 |
| 1.8 | -1.52753 | -1.52770 | -1.52753 |
| 2.0 | -1.58114 | -1.58124 | -1.58114 |

***Table 2.*** *Numerical values of the reduced skin-friction coefficient, local Nusselt number, and local Sherwood number for varying thermal Biot numbers and Dufour parameter.*

| $Bi_1$ | $Bi_2$ | $Df$ | $C_f Re_x^{1/2}$ | $Nu_x Re_x^{-1/2}$ | $Sh_x Re_x^{-1/2}$ |
|---|---|---|---|---|---|
| 0.5 | 0.5 | 0.4 | -0.74483965 | 0.191249 | 0.221236 |
| 0.5 | | | -0.74483965 | 0.191249 | 0.221236 |
| 1 | | | -0.6225689 | 0.248921 | 0.206965 |

| $Bi_1$ | $Bi_2$ | $Df$ | $C_f Re_x^{1/2}$ | $Nu_x Re_x^{-1/2}$ | $Sh_x Re_x^{-1/2}$ |
|---|---|---|---|---|---|
| 2 | | | -0.52738027 | 0.291415 | 0.19724 |
| | 0.5 | | -0.74483965 | 0.191249 | 0.221236 |
| | 1 | | -0.69213595 | 0.183588 | 0.314294 |
| | 2 | | -0.64523425 | 0.176666 | 0.398565 |
| | | 0.4 | -0.74483965 | 0.191249 | 0.221236 |
| | | 0.8 | -0.70774344 | 0.172766 | 0.233399 |
| | | 1.2 | -0.66855528 | 0.150691 | 0.247875 |

***Table 3.*** *Numerical values of the reduced skin-friction coefficient, local Nusselt number, and local Sherwood number for varying* $Ec, M, R$.

| $Ec$ | $M$ | $R$ | $C_f Re_x^{1/2}$ | $Nu_x Re_x^{-1/2}$ | $Sh_x Re_x^{-1/2}$ |
|---|---|---|---|---|---|
| 0.5 | 0.5 | 0.4 | -0.74483965 | 0.191249 | 0.221236 |
| 0.2 | | | -0.74483965 | 0.191249 | 0.221236 |
| 0.4 | | | -0.72166608 | 0.178459 | 0.229087 |
| 0.6 | | | -0.69969606 | 0.166606 | 0.236329 |
| | 0.2 | | -0.64440687 | 0.197144 | 0.221235 |
| | 0.4 | | -0.74483965 | 0.191249 | 0.221236 |
| | 0.6 | | -0.8385522 | 0.185363 | 0.221462 |
| | | 0.4 | -0.74483965 | 0.191249 | 0.221236 |
| | | 0.8 | -0.68576124 | 0.170661 | 0.234171 |
| | | 1.2 | -0.6407977 | 0.155945 | 0.243598 |

***Table 4.*** *Numerical values of the reduced skin-friction coefficient, local Nusselt number, and local Sherwood number for varying* $\theta_w, Q, Nb, Nt$.

| $\theta_w$ | $Q$ | $Nb$ | $Nt$ | $C_f Re_x^{1/2}$ | $Nu_x Re_x^{-1/2}$ | $Sh_x Re_x^{-1/2}$ |
|---|---|---|---|---|---|---|
| 0.5 | 0.5 | 0.8 | 0.8 | -0.74483965 | 0.191249 | 0.221236 |
| 1.2 | | | | -0.74483965 | 0.191249 | 0.221236 |
| 1.4 | | | | -0.72017215 | 0.180902 | 0.227303 |
| 1.6 | | | | -0.6909948 | 0.169255 | 0.234042 |
| | 0.2 | | | -0.74483965 | 0.191249 | 0.221236 |
| | 0.4 | | | -0.61197965 | 0.130959 | 0.257429 |
| | 0.6 | | | -0.38669165 | 0.034938 | 0.312166 |
| | | 0.5 | | -0.72412 | 0.200801 | 0.187354 |
| | | 0.8 | | -0.74484 | 0.191249 | 0.221236 |
| | | 1.5 | | -0.74943 | 0.179588 | 0.246462 |
| | | | 0.5 | -0.7701 | 0.191208 | 0.237908 |
| | | | 0.8 | -0.74484 | 0.191249 | 0.221236 |

| $\theta_w$ | $Q$ | $Nb$ | $Nt$ | $C_f Re_x^{1/2}$ | $Nu_x Re_x^{-1/2}$ | $Sh_x Re_x^{-1/2}$ |
|---|---|---|---|---|---|---|
| | | | 1.5 | -0.68726 | 0.189975 | 0.186077 |

## 3. Results and Discussion

This study considers radiative heat transmission, cross-diffusion (Soret and Dufour effects), thermophoresis, internal heat production, and convective boundary conditions in magnetohydrodynamic nonlinear convection flow of a Jeffrey nanofluid across a vertical surface. Key dimensionless parameters are examined in detailed parametric research. For the numerical scheme validation, the calculated skin-friction coefficient $f''(0)$ is compared with the results of Dalir [6] using the implicit Keller-box method, and Hayat et al. [5] employing homotopy analysis for a limit. The excellent consistency in Table 1 supports the present computational strategy. Figure 2 shows how the Dufour parameter impacts velocity, temperature, and concentration distributions. Increased Dufour number means both increased fluid velocity and temperature profiles, while the concentration field decreases. The Dufour effect increases heat flow from concentration gradients, increasing thermal energy in the boundary layer and decreasing species concentration.

Figure 3 shows how changing the Soret parameter affects velocity and concentration profiles. Increasing the Soret value shows higher thermally induced mass diffusion in the boundary layer. In Figure 4, the impact of the Deborah number on the dimensionless velocity $f'(\chi)$, temperature $\theta(\chi)$, and concentration $\phi(\chi)$ is presented. Increasing $\beta$ increases the velocity profile but decreases the temperature and concentration profile. Physically, a larger Deborah number indicates more pronounced elastic effects concerning the fluid's relaxation properties; that is, flow resistance is diminished, and fluid flow is expedited, which results in a reduction in the thermal and concentration boundary layers. Figure 5 shows the velocity profile due to the magnetic parameter (M). It is observed that dominant magnetic effects retard fluid flow due to the Lorentz force opposing the flow.

Figures 6 and 7 depict the effects of the radiation parameter $R$ and the temperature ratio parameter $\theta_w$, respectively, on the flow characteristics. It is observed that increasing either parameter enhances both the velocity and temperature distributions within the boundary layer. Physically, stronger thermal radiation or a higher surface-to-ambient temperature ratio elevates the energy level of the fluid, which reduces thermal resistance and accelerates the flow. In contrast, the concentration profile decreases with higher values of $R$ and $\theta_w$, as intensified thermal effects weaken the concentration boundary layer and promote mass diffusion away from the surface. Figure 8 presents the impact of the heat generation parameter $Q$ on the flow behavior. An increase in $Q$ signifies stronger internal heat production within the fluid, which elevates the temperature distribution across the boundary layer. The resulting rise in thermal energy intensifies buoyancy effects, thereby promoting fluid motion and increasing the velocity and temperature profiles.

Figures 9 and 10 demonstrate how thermal and solutal Biot numbers, $Bi_1$ and $Bi_2$, affect velocity, temperature, and concentration curves. Increased Biot numbers and parameter values boost boundary surface convective heat and mass transport, strengthening fluid and boundary layer interactions. Thus, momentum, temperature, and concentration boundary layers increase. These results show that convective boundary conditions strongly limit engineering heat and mass transport. Figure 11 illustrates the effect of the convection parameter on the dimensionless velocity $f'(\chi)$, temperature $\theta(\chi)$, and concentration $\phi(\chi)$ profiles. An increase in convection parameters is shown to enhance velocity distribution; however, both temperature and concentration profiles decline. A physically stronger convection parameter results in an increase in buoyancy-driven flow, which means an increase in the rate of fluid motion within the boundary layer. Stronger fluid movement accelerates heat and mass transfer away from the surface, thins thermal and concentration boundary layers, and lowers temperature and concentration profiles.

Figures 12 and 13 show how the Brownian motion parameter $Nb$ and the thermophoresis parameter $Nt$ affect velocity, temperature, and concentration distributions. The parameters regulate nanoparticle diffusion and temperature-gradient-induced particle migration, which modifies thermal and concentration-boundary-layer properties, making them crucial to nanofluid transport. An increase in $Nb$ means there is more random motion of nanoparticles that results in stronger energy interactions between the fluid and the suspended particles, leading to more thermal diffusion and an upward shift in the temperature profile. The concentration profile, however, is expected to be lower because of induced particle migration away from the boundary surface. Due to the energy increase within the boundary layer, the velocity field is likely to improve. On the contrary, the thermophoresis parameter $Nt$ signifies the temperature-gradient-induced migration of nanoparticles. A greater $Nt$ value shifts nanoparticles away from the boundary surface towards the surrounding less hot fluid, causing an increase in the temperature and concentration boundary layer thickness. Increasing thermal energy owing to thermophoretic effect intensification should enhance fluid velocity. In nanofluid flow systems, the interaction of $Nb$ and $Nt$ alters the random motion and

diffusion of the nanoparticles, as well as the thermophoretic transport of the nanoparticles.

## 4. Concluding Remarks

This work investigated the magnetohydrodynamic nonlinear convection flow of a Jeffrey nanofluid across a vertical extending surface under radiation, internal heat production, Brownian motion, thermophoresis, cross-diffusion effects, and convective boundary conditions. The analysis reveals that some parameters of nonlinear convection and magneto convection influence the momentum boundary layers of the flow structure the most. In contrast, the Deborah number changes the viscoelastic response, which has a fundamental influence on the profiles of the flow structure. The temperature field, enhanced by thermal radiation, temperature ratio, and heat source, overpowers and accelerates buoyancy-driven forces when combined with diffusion effects like Soret and Dufour. Boundancy-driven heat and mass transfers are dominated by Soret and Dufour effects. The Brownian motion increases heat energy owing to nanoparticle random motion, while concentration falls, and thermophoresis raises temperature and concentration layers, causing particles to travel along thermal gradients. The thermally and concentration active layers increase with the enhanced surface psi flow, with the increased thermal and solutal Biot numbers strengthening the surface convection layers.

Overall, Magnetic forces, viscoelasticity, nonlinear buoyancy, nanoparticle transport, and cross-diffusion mechanisms regulate flow and heat-mass transfer, providing insight for advanced thermal engineering and nanofluid-based industrial applications.

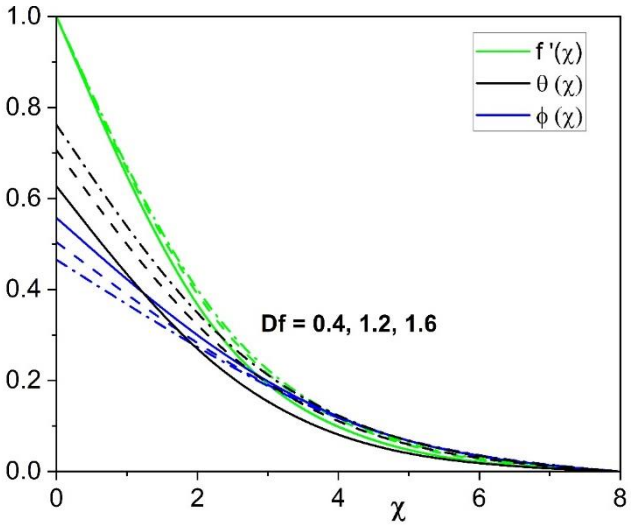


*Figure 2. Influence of Dufour number on $f'(\chi), \theta(\chi)$ and $\phi(\chi)$.*

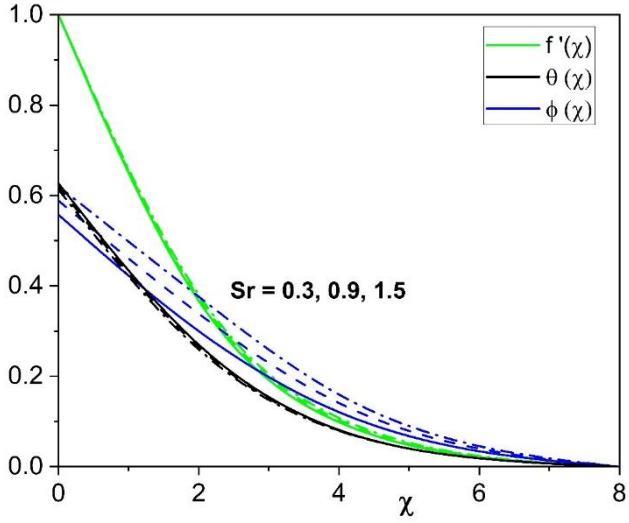


*Figure 3. Influence of Soret number on $f'(\chi), \theta(\chi)$ and $\phi(\chi)$.*

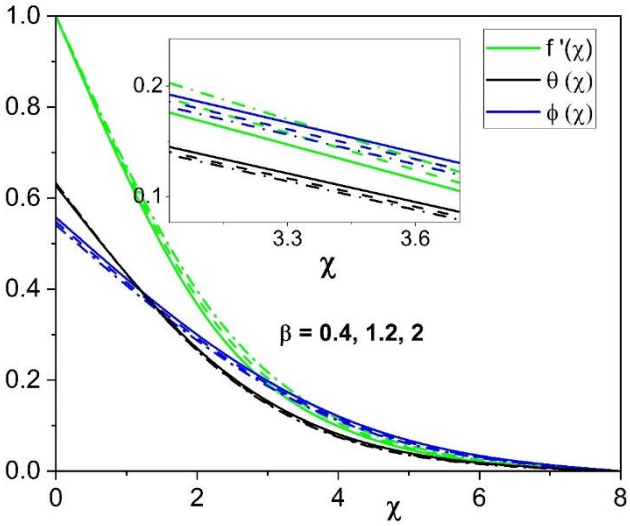


*Figure 4. Influence of Deborah number on $f'(\chi), \theta(\chi)$ and $\phi(\chi)$.*

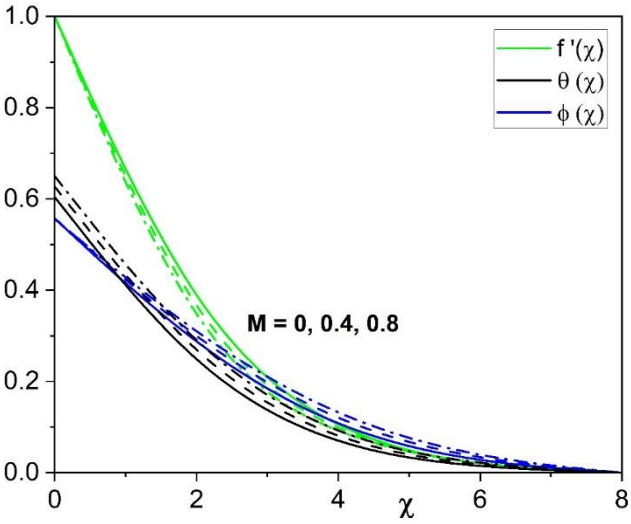


*Figure 5. Influence of magnetic field on $f'(\chi), \theta(\chi)$ and $\phi(\chi)$.*

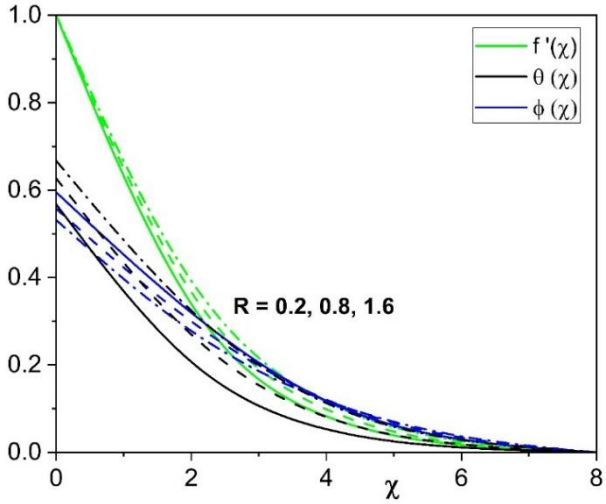


***Figure 6.*** *Influence of thermal radiation on* $f'(\chi), \theta(\chi)$ *and* $\phi(\chi)$.

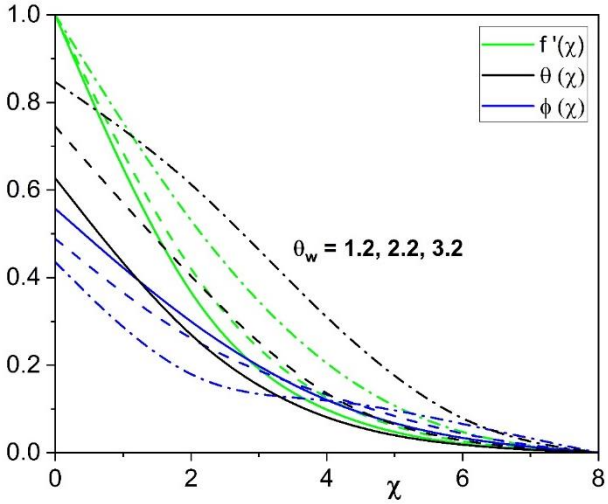


***Figure 7.*** *Influence of temperature ratio parameter on* $f'(\chi), \theta(\chi)$ *and* $\phi(\chi)$.

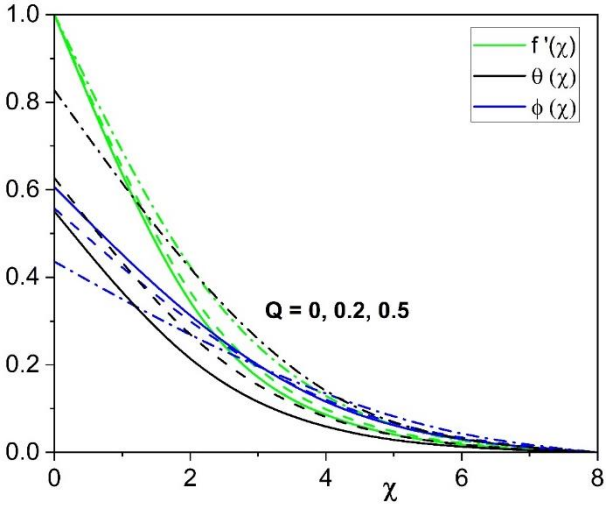


***Figure 8.*** *Influence of heat source parameter on* $f'(\chi), \theta(\chi)$ *and* $\phi(\chi)$.

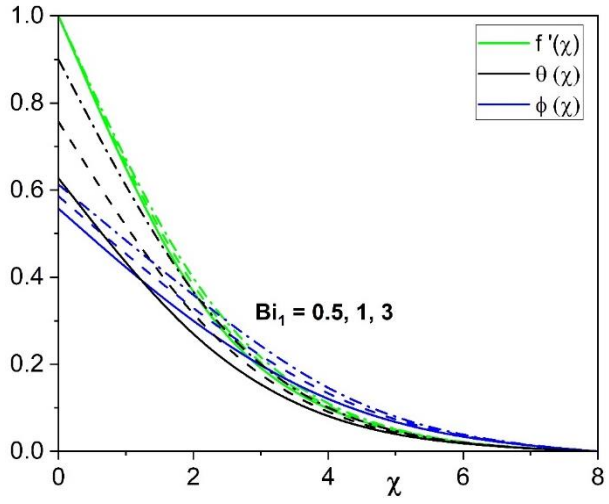


***Figure 9.*** *Influence of thermal Biot number on* $f'(\chi), \theta(\chi)$ *and* $\phi(\chi)$.

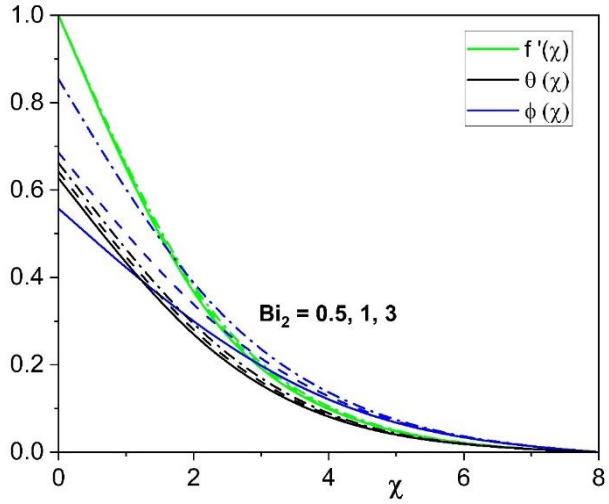


***Figure 10.*** *Influence of concentration Biot number on* $f'(\chi), \theta(\chi)$ *and* $\phi(\chi)$.

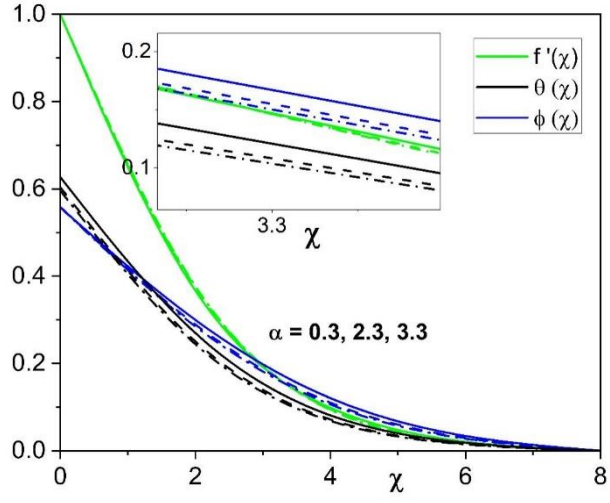


***Figure 11.*** *Influence of convection parameter on* $f'(\chi), \theta(\chi)$ *and* $\phi(\chi)$.

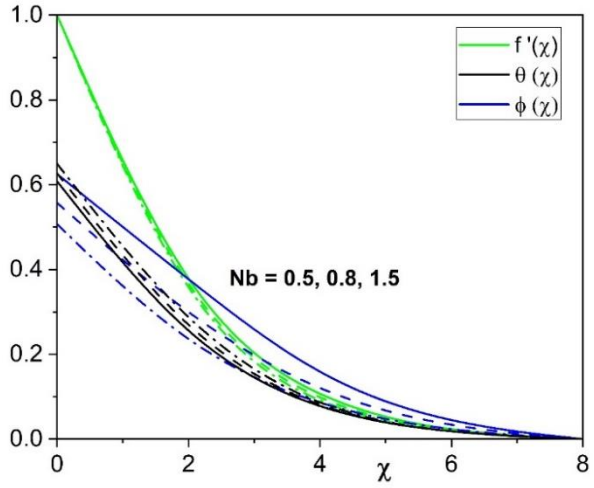


*Figure 12. Influence of convection parameter on $f'(\chi), \theta(\chi)$ and $\phi(\chi)$.*

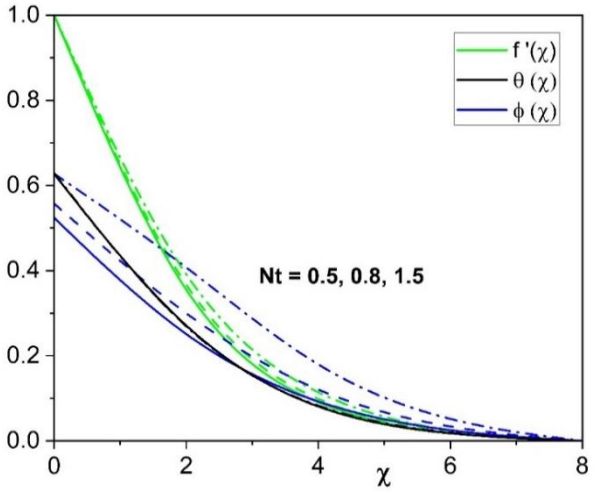


*Figure 13. Influence of convection parameter on $f'(\chi), \theta(\chi)$ and $\phi(\chi)$.*

## Abbreviations

| | |
|---|---|
| PDEs | Partial Differential Equations |
| ODEs | Ordinary Differential Equations |
| $\lambda$ | Mixed Convection Parameter |
| $Gr_x$ | Local Grashof Number |
| $Re_x$ | Local Reynolds Number |
| $\beta$ | Nonlinear Convection Parameter |
| $\alpha$ | Thermal Buoyancy Parameter |
| $N$ | Buoyancy Ratio Parameter |
| $M$ | Magnetic Parameter |
| $D_f$ | Dufour Parameter |
| $Pr$ | Prandtl Number |
| $Q$ | Heat Generation/Absorption Parameter |
| $R$ | Thermal Radiation Parameter |
| $\theta_w$ | Temperature Ratio Parameter |
| $Ec$ | Eckert Number |
| $Sc$ | Schmidt Number |
| $\tau$ | Thermophoretic Parameter |
| $Sr$ | Soret Parameter |
| $S$ | Suction/Injection Parameter |
| $Bi_1$ | Thermal Biot Number |
| $Bi_2$ | Concentration Biot Number |
| $N_b$ | Brownian Motion Parameter |
| $N_t$ | Thermophoresis Parameter |
| $\sigma$ | Electrical Conductivity |
| $\rho$ | Fluid Density |
| $\nu$ | Kinematic Viscosity |
| $k$ | Thermal Conductivity |

## Author Contributions

**Sunitha Manchaiah Savithramma:** Data curation, Formal Analysis, Investigation, Writing – original draft

**Kemparaju Siddegowda:** Methodology, Software, Validation, Visualization

**Jagadeesha Ragibychanahalli Devaraju:** Project administration, Software, Supervision

**Sampath Kumar Poojari Borappa:** Formal Analysis, Supervision, Writing – review & editing

## Conflicts of Interest

The authors declare no conflicts of interest.

## References

[1] M. Turkyilmazoglu and I. Pop, "Soret and heat source effects on the unsteady radiative MHD free convection flow from an impulsively started infinite vertical plate," International Journal of Heat and Mass Transfer, 55(25–26) (2012) 7635–7644. https://doi.org/10.1016/j.ijheatmasstransfer.2012.07.079

[2] Lian-Cun Zheng, Xin Jin, Xin-Xin Zhang, and Jun-Hong Zhang, "Unsteady heat and mass transfer in MHD flow over an oscillatory stretching surface with Soret and Dufour effects," Acta Mechanica Sinica, 29(5) (2013) 667–675. https://doi.org/10.1007/s10409-013-0066-6

[3] P. Sudarsana Reddy and Ali J. Chamkha, "Soret and Dufour effects on MHD convective flow of $Al_2O_3$–water and $TiO_2$–water nanofluids past a stretching sheet in porous media with heat generation/absorption," Advanced Powder Technology, 27(4) (2016) 1207–1218. https://doi.org/10.1016/j.apt.2016.04.005

[4] P. B. Sampath Kumar, B. J. Gireesha, B. Mahanthesh, and R. S. R. Gorla, "Nonlinear thermal convection in Jeffrey liquid flow with cross diffusion effects past a stretched surface," Diffusion Foundations, 11 (2017) 84–98. https://doi.org/10.4028/www.scientific.net/df.11.84

[5] Tasawar Hayat, Ikram Ullah, Taseer Muhammad, and Ahmed Alsaedi, "Radiative three-dimensional flow with Soret and Dufour effects," International Journal of Mechanical Sciences, 133 (2017) 829–837. https://doi.org/10.1016/j.ijmecsci.2017.09.015

[6] Q. M. Zaigham Zia, Ikram Ullah, Metal Waqas, A. Alsaedi, and T. Hayat, "Cross diffusion and exponential space dependent heat source impacts in radiated three-dimensional flow of Casson fluid by heated surface," Results in Physics, 8 (2018) 1275–1282. https://doi.org/10.1016/j.rinp.2018.01.001

[7] R. Madan Kumar, R. Srinivasa Raju, M. Anil Kumar, and B. Venkateswarlu, "A numerical study of thermal and diffusion effects on MHD Jeffrey fluid flow over a porous stretching sheet with activation energy," Numerical Heat Transfer, Part A: Applications, 86(13) (2025) 4423–4444. https://doi.org/10.1080/10407782.2024.2319344

[8] Subhan Ullah, Ikram Ullah, Amir Ali, Kamal Shah, and Thabet Abdeljawad, "Investigation of cross-diffusion effect on radiative Jeffery–Hamel flow in convergent/divergent stretchable channel with Lorentz force and Joule heating," Alexandria Engineering Journal, 86 (2024) 289–297. https://doi.org/10.1016/j.aej.2023.11.054

[9] J. V. Ramana Reddy, K. Anantha Kumar, V. Sugunamma, and N. Sandeep, "Effect of cross diffusion on MHD non-Newtonian fluids flow past a stretching sheet with non-uniform heat source/sink: A comparative study," Alexandria Engineering Journal, 57(3) (2018) 1829–1838. https://doi.org/10.1016/j.aej.2017.03.008

[10] Gadamsetty Revathi, Mamatha S. Upadhya, Raghunath Kodi, Dhananjay Yadav, Haribabu Kommaddi, and M. Jayachandra Babu, "Influence of cross-diffusion, couple stress, and non-Fourier heat flux on Jeffrey hybrid nanofluid flow and entropy generation in a vertical cylinder," Phase Transitions, (2025) 1–22. https://doi.org/10.1080/01411594.2025.2536187

[11] Saima Noreen, Areeba Riaz, and Dianchen Lu, "Soret–Dufour effects in electroosmotic biorheological flow of Jeffrey fluid," Heat Transfer, 49(4) (2020) 2355–2374. https://doi.org/10.1002/htj.21725

[12] C. S. K. Raju and N. Sandeep, "Heat and mass transfer in MHD non-Newtonian bio-convection flow over a rotating cone/plate with cross diffusion," Journal of Molecular Liquids, 215 (2016) 115–126.

[13] B. Shilpa, V. Leela, B. C. Prasannakumara, and Pulla Nagabhushana, "Soret and Dufour effects on MHD double-diffusive mixed convective heat and mass transfer of couple stress fluid," Waves in Random and Complex Media, 35(6) (2025) 10980–11001. https://doi.org/10.1080/17455030.2022.2119491

[14] Mair Khan, T. Salahuddin, Muhammad Awias, Basem Al Awan, Muyassar Norberdiyeva, and Nidhal Ben Khedher, "Soret and Dufour effects of Bingham plastic fluid flow over a solar radiative heat flux," Dynamics of Atmospheres and Oceans, (2025) 101600. https://doi.org/10.1016/j.dynatmoce.2025.101600

[15] Surbhi Sharma, Mamta Goyal, and Amit Dadheech, "Melting, Soret and Dufour effect on MHD Casson fluid flow over a stretching sheet with slip conditions," Journal of Engineering Mathematics, 146(1) (2024) 18. https://doi.org/10.1007/s10665-024-10364-0

[16] Rama Subba Reddy Gorla and Ibrahim Sidawi, "Free convection on a vertical stretching surface with suction and blowing," Applied Scientific Research, 52(3) (1994) 247–257. https://doi.org/10.1007/bf00853952

[17] T. Y. Wang, "Mixed convection heat transfer from a vertical plate to non-Newtonian fluids," International Journal of Heat and Fluid Flow, 16 (1995) 56–61. https://doi.org/10.1016/0142-727x(94)00008-z

[18] Ali J. Chamkha, "Hydromagnetic three-dimensional free convection on a vertical stretching surface with heat generation or absorption," International Journal of Heat and Fluid Flow, 20 (1999) 84–92. https://doi.org/10.1016/s0142-727x(98)10032-2

[19] Mohammad Mehdi Rashidi, Muhammad Ashraf, Behnam Rostami, Taher Mohammad Rastegari, and Sumra Bashir, "Mixed convection boundary-layer flow of a micropolar fluid towards a heated shrinking sheet by homotopy analysis method," Thermal Science, 20(1) (2016) 21–34. https://doi.org/10.2298/tsci130212096r

[20] B. J. Gireesha, B. Mahanthesh, Rama Subba Reddy Gorla, and K. L. Krupalakshmi, "Mixed convection two-phase flow of Maxwell fluid under the influence of nonlinear thermal radiation and non-uniform heat source/sink," Ain Shams Engineering Journal, 9(4) (2018) 735–746. https://doi.org/10.1016/j.asej.2016.04.020

[21] F. M. Ali, R. Nazar, N. M. Arifin, and I. Pop, "Mixed convection stagnation-point flow on a vertical stretching sheet with external magnetic field," Applied Mathematics and Mechanics, 35(2) (2014) 155–166. https://doi.org/10.1007/s10483-014-1780-8

[22] M. Y. Malik, I. Khan, A. Hussain, and T. Salahuddin, "Mixed convection flow of MHD Eyring–Powell nanofluid over a stretching sheet: A numerical study," AIP Advances, 5 (2015) 117–118. https://doi.org/10.1063/1.4935639

[23] B. Mahanthesh, B. J. Gireesha, and R. S. R. Gorla, "Heat and mass transfer effects on the mixed convective flow of chemically reacting nanofluid past a moving/stationary vertical plate," Alexandria Engineering Journal, 55(1) (2016) 569–581. https://doi.org/10.1016/j.aej.2016.01.022

[24] S. Das, R. N. Jana, and O. D. Makinde, "Mixed convective magnetohydrodynamic flow in a vertical channel filled with nanofluids," Engineering Science and Technology, an International Journal, 18(2) (2015) 244–255. https://doi.org/10.1016/j.jestch.2014.12.009

[25] K. Vajravelu, J. R. Cannon, J. Leto, R. Semmoum, N. Nathan, M. Draper, and D. Hammock, "Nonlinear convection at a porous flat plate with application to heat transfer from a dike," Journal of Mathematical Analysis and Applications, 277 (2003) 609–623. https://doi.org/10.1016/s0022-247x(02)00634-0

[26] P. K. Kameswaran, P. Sibanda, M. K. Partha, and P. V. S. N. Murthy, "Thermophoretic and non-linear convection in non-Darcy porous medium," Journal of Heat Transfer, 136(4) (2014) 042601. https://doi.org/10.1115/1.4025902

[27] S. Shaw, G. Mahanta, and P. Sibanda, "Non-linear thermal convection in a Casson fluid flow over a horizontal plate with convective boundary condition," Alexandria Engineering Journal, 55(2) (2016) 1295–1304. https://doi.org/10.1016/j.aej.2016.04.020

[28] D. K. Jyoti, V. Nagaradhika, P. B. Sampath Kumar, and Ali J. Chamkha, "Nonlinear convection and radiative heat transfer in kerosene–alumina nanofluid flow between two parallel plates with variable viscosity," Journal of Nanofluids, 13(5) (2024) 1055–1062. https://doi.org/10.1166/jon.2024.2193

[29] Muhammad Shoaib, Shafaq Naz, Muhammad Asif Zahoor Raja, Khadeeja Arshad, Iftikhar Ahmad, and Kottakkaran Sooppy Nisar, "Numerical treatment for nonlinear mixed convection and thermal radiative Newtonian fluid flow system," Journal of Radiation Research and Applied Sciences, 18(3) (2025) 101675. https://doi.org/10.1016/j.jrras.2025.101675

[30] S. Ramesh Krishnan, "Rheometric analysis of impact of temperature, volume fraction and mass of nanoparticle on the viscosity of water based nanofluids," Asian Review of Mechanical Engineering, 12(1) (2023) 44–49. https://doi.org/10.51983/arme-2023.12.1.3669

[31] M. S. Sunitha, S. Kemparaju, R. D. Jagadeesha, and P. B. Sampath Kumar, "Comparative performance analysis of Cu and $Fe_3O_4$ nanofluids in heat transfer applications," Asian Review of Mechanical Engineering, 14(1) (2025) 39–50. https://doi.org/10.70112/arme-2025.14.1.4287

[32] S. V. Nishandar, Vivek Prabhu, Sandeep Deshpande, Vallabh Apate, Sushant Padalkar, and Avesahemad Husainy, "Performance enhancement of a vapor compression refrigeration system using $Al_2O_3$, CuO, and hybrid nanoparticles," Asian Review of Mechanical Engineering, 14(1) (2025) 1–7. https://doi.org/10.70112/arme-2025.14.1.4282

[33] G. Ramasekhar, S. Jakeer, S. R. R. Reddy, S. Alkarni, and N. A. Shah, "Biomedical importance of Casson nanofluid flow with silver and Fe2O3 nanoparticles delivered into a stenotic artery: Numerical study," AIMS Mathematics, 9(8) (2024) 23142–23157. https://doi.org/10.3934/math.20241125

[34] G. Ramasekhar and P. B. A. Reddy, "Numerical analysis of significance of multiple shape factors in Casson hybrid nanofluid flow over a rotating disk," International Journal of Modern Physics B, 37(12) (2023) 2350113. https://doi.org/10.1142/S0217979223501138

[35] G. Ramasekhar, "Artificial neural network and numerical simulation for magneto hydrodynamics hybrid nanofluid flow towards a stretching cylinder," Journal of Nanofluids, 13(3) (2024) 760–771. https://doi.org/10.1166/jon.2024.2177

[36] T. Hayat, Z. Iqbal, M. Mustafa, and A. Alsaedi, "Unsteady flow and heat transfer of Jeffrey fluid over a stretching sheet," Thermal Science, 18(4) (2014) 1069–1078. https://doi.org/10.2298/tsci110907092h

[37] M. Nandini, G. Saini, S. V. K. Varma, J. V. Tawade, N. V. Satpute, R. Ghodhbani, G. Rasool, M. Gupta, and M. I. Khan, "Non-linear thermal radiation impacts on MHD nanofluid flow in a rotating channel with Darcy-Forchheimer model: An entropy analysis," Journal of Radiation Research and Applied Sciences, 18(1) (2025) 101228. https://doi.org/10.1016/j.jrras.2024.101228

[38] D. Lu, M. Ramzan, N. ul Huda, J. D. Chung, and U. Farooq, "Nonlinear radiation effect on MHD Carreau nanofluid flow over a radially stretching surface with zero mass flux at the surface," Scientific Reports, 8(1) (2018) 3709. https://doi.org/10.1038/s41598-018-22000-w

[39] K. Anantha Kumar, A. C. Venkata Ramudu, V. Sugunamma, and N. Sandeep, "Effect of non-linear thermal radiation on MHD Casson fluid flow past a stretching surface with chemical reaction," International Journal of Ambient Energy, 43(1) (2022) 8400–8407. https://doi.org/10.1080/01430750.2022.2097947

[40] K. Sreelatha, J. Girish Kumar, and P. V. Satyanarayana, "Influence of nonlinear radiation on MHD nanofluid flow over a cone with second-order velocity and thermal slips: A numerical study," Heat Transfer, 51(8) (2022) 8043–8064. https://doi.org/10.1002/htj.22680

[41] A. I. Jaafar, I. Waini, A. Jamaludin, R. Nazar, and I. Pop, "MHD flow and heat transfer of a hybrid nanofluid past a nonlinear surface stretching/shrinking with effects of thermal radiation and suction," Chinese Journal of Physics, 79 (2022) 13–27. https://doi.org/10.1016/j.cjph.2022.06.026

[42] N. Dalir, "Numerical study of entropy generation for forced convection flow and heat transfer of a Jeffrey fluid over a stretching sheet," Alexandria Engineering Journal, (2014). https://doi.org/10.1016/j.aej.2014.08.005

[43] M. Qasim, "Heat and mass transfer in a Jeffrey fluid over a stretching sheet with heat source/sink," Alexandria Engineering Journal, 52(4) (2013) 571–575. https://doi.org/10.1016/j.aej.2013.08.004

[44] S. A. Shehzad, F. E. Alsaadi, S. J. Monaquel, and T. Hayat, "Soret and Dufour effects on the stagnation point flow of Jeffrey fluid with convective boundary condition," European Physical Journal Plus, 128 (2013) 56. https://doi.org/10.1140/epjp/i2013-13056-6

[45] G. K. Ramesh, "Numerical study of the influence of heat source on stagnation point flow towards a stretching surface of a Jeffrey nanoliquid," Journal of Engineering, (2015) 382061. https://doi.org/10.1155/2015/382061

[46] M. Veera Krishna and Ali J. Chamkha, "Hall and ion slip effects on magnetohydrodynamic convective rotating flow of Jeffreys fluid over an impulsively moving vertical plate embedded in a porous medium," Numerical Methods for Partial Differential Equations, 37(3) (2021) 2150–2177. https://doi.org/10.1002/num.22670